Accepted for publication by AJ
Preprint typeset using LaTeX style emulateapj v. 5/2/11

arXiv:1601.03056v1 [astro-ph.GA] 12 Jan 2016

A CONSTRAINT ON QUASAR CLUSTERING AT $Z = 5$ FROM A BINARY QUASAR

Ian D. McGreer[1], Sarah Eftekharzadeh[2], Adam D. Myers[2], and Xiaohui Fan[1]

Accepted for publication by AJ

ABSTRACT

We report the discovery of a quasar pair at $z = 5$ separated by $21''$. Both objects were identified as quasar candidates using simple color selection techniques applied to photometric catalogs from the CFHT Legacy Survey (CFHTLS). Spectra obtained with the MMT present no discernible offset in redshift between the two objects; on the other hand, there are clear differences in the emission line profiles and in the multiwavelength spectral energy distributions that strongly disfavor the hypothesis that they are gravitationally lensed images of a single quasar. Both quasars are surprisingly bright given their proximity (a projected separation of ~ 135 kpc), with $i = 19.4$ and $i = 21.4$. Previous measurements of the luminosity function demonstrate that luminous quasars are extremely rare at $z = 5$; the existence of this pair suggests that quasars have strong small-scale clustering at high redshift. Assuming a real-space correlation function of the form $\xi(r) \propto (r/r_0)^{-2}$, this discovery implies a correlation length $r_0 \gtrsim 20h^{-1}\,\mathrm{Mpc}$, consistent with a rapid strengthening of quasar clustering at high redshift as seen in previous observations and predicted by theoretical models where feedback effects are inefficient at shutting down black hole growth at high redshift.

Subject headings: quasars: general — quasars: individual (CFHTLS J022112.61-034252.1, CFHTLS J022112.31-034231.6) — galaxies: halos

1. INTRODUCTION

The discovery that luminous quasars cluster strongly at redshifts approaching $z \sim 4$ (with a scale length of $r_0 \sim 25\,h^{-1}\,\mathrm{Mpc}$; Shen et al. 2007) potentially poses an interesting cosmological challenge. It could be that quasar clustering strongly declines with luminosity at high redshift, meaning that current samples only trace the most strongly clustered sources. But, faint quasars do not appear to cluster significantly more weakly than bright quasars at $z \sim 2.5$ (White et al. 2012; Eftekharzadeh et al. 2015) or below (e.g. da Ângela et al. 2008; Shen et al. 2009, 2013). Thus, if quasar clustering is highly luminosity-dependent at $z \sim 4.5$, then quasars (as a population) would have to alter rapidly over 10% of the Hubble Time, then change more quiescently over the final 80% of cosmic history. Further, most models invoke a narrow range of halo mass for a wide range of quasar luminosity in order to reproduce the quasar luminosity function (e.g., Lidz et al. 2006; see also the discussion in Appendix B of White et al. 2012).

Alternatively, quasars at high redshift could simply trace the growth of their parent dark matter halos while they are actively accreting. Such a scenario essentially represents the maximal possible increase in clustering amplitude with redshift; under scenarios other than this "maximal growth" model the correlation length of quasars should eventually diminish at high redshift. Fig. 13 of Hopkins et al. (2007) illustrates this point — quasar clustering should decrease at $z > 4$ for scenarios in which quasars are efficiently quenched.

Observations of quasar clustering at $z > 4$ are currently limited to relatively small samples of highly luminous quasars (Shen et al. 2007). Improving this situation is a significant challenge, given that it requires expensive spectroscopic campaigns targeting faint candidates at low sky density ($\sim$1 deg^{-2}). One promising avenue is the study of pairs of quasars that are separated by both a small angle on the plane of the sky and by a small velocity window in redshift space. Such pairs, often called "binary quasars" in the literature, are sufficiently rare to confirm with dedicated spectroscopic follow-up, but have a very strong clustering strength. Binary quasars can therefore be used to estimate the correlation length of quasar clustering even using small samples (e.g. Hennawi et al. 2006; Myers et al. 2008; Shen et al. 2010). Of order a dozen $z \sim 4$ binary quasars with proper separations of less than ~ 1 Mpc are currently known (e.g. Hennawi et al. 2010).

The highest redshift binary quasar discovered to date is a quasar pair at $z = 4.26$ separated by $33''$, or about 230 kpc proper, on the plane of the sky (Schneider et al. 2000). The pair was discovered serendipitously—while spectroscopically confirming an $i = 20.4$ quasar candidate a second $i = 21.3$ quasar at the same redshift happened to be located in the slit. This single quasar pair was sufficient to ascertain that $z \sim 4.25$ quasars cluster with a correlation length of $r_0 \sim 10$–$30\,\mathrm{Mpc}$, an observation later confirmed using much larger samples by Shen et al. (2007). In this paper, we present a similar find. During a survey of $4.7 \lesssim z \lesssim 5.2$ quasar candidates, we have discovered a quasar pair separated by $21''$, or about 135 kpc proper. In this paper, we discuss the discovery of this pair, our reasoning for why it is a binary quasar (rather than a gravitational lens) and the implications of such a pair for quasar clustering at $z \sim 5$. All quoted magnitudes are on the AB system (Oke

Observations reported here were obtained at the MMT Observatory, a joint facility of the Smithsonian Institution and the University of Arizona.

imcgreer@as.arizona.edu
[1] Steward Observatory, 933 North Cherry Avenue, Tucson, AZ 85721, USA.
[2] Department of Physics and Astronomy, University of Wyoming, Laramie, WY 82071, USA.

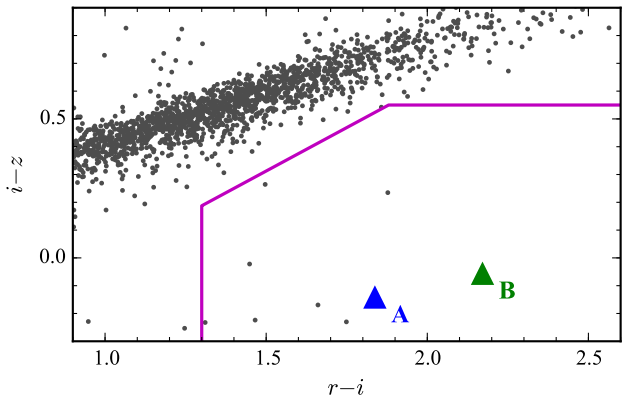

Figure 1. Color-color plot displaying the color cuts used to select $z \sim 5$ quasar candidates (magenta line). The gray points are objects from the CFHTLS-Wide that pass our morphological and quality cuts and that are located in the same 1 deg^2 patch as the quasar pair. The blue symbol denotes QSO-A and the green symbol QSO-B. Error bars are smaller than the symbol size; the colors are clearly different although both are well within our selection boundary.

& Gunn 1983) and corrected for Galactic extinction using the dust maps of Schlegel et al. (1998). We adopt a cosmology of $(\Omega_{\rm m}, \Omega_\Lambda, h \equiv H_0/100\,{\rm km\,s^{-1}\,Mpc^{-1}}) = (0.307, 0.693, 0.677)$ consistent with recent results from *Planck* (Planck Collaboration et al. 2015).

2. OBSERVATIONS

2.1. *Initial Selection from CFHTLS-W1*

In previous work, we measured the $z = 5$ quasar luminosity function (QLF) using quasars selected from the SDSS Stripe 82 region to a depth of $i = 22$ (McGreer et al. 2013). We are extending this work to fainter quasars using the CFHTLS-Wide survey (Gwyn 2012). The full CFHTLS-Wide encompasses four fields with a total area of 150 deg^2 and includes five optical bands, *ugriz*. We downloaded the publicly available stacked images[3] and generated object catalogs using SExtractor (Bertin & Arnouts 1996). The catalogs include PSF photometry derived from the PSFEx models provided by the CFHTLS. We included two of the CFHT-Wide fields in the selection described here; W1 at 02:18 -07:00 and W3 at 14:18 +54:30.

Full details of our faint $z \sim 5$ quasar selection will be provided in a future work. Briefly, we use the difference between the elliptical Kron aperture magnitude (MAG_AUTO) flux measurements and the PSF flux measurement (MAG_PSF) from SExtractor to obtain a rough star/galaxy separation. Through various tests we found that requiring MAG_AUTO − MAG_PSF > -0.15 is highly complete to point sources to a limit of $i < 23$, while greatly reducing contamination from compact galaxies. We further apply a number of quality cuts. First, we require clean photometry SExtractor FLAGS <= 4. Second, we remove objects lying within the masked regions (generally due to bright stars) as provided by the CFHTLS; this reduces our effective area by $\sim 1\%$. Finally, we remove CFHTLS fields for which the stellar locus is poorly matched to a reference locus derived from the CFHTLS-Deep survey, indicating issues with the photometric calibration. This reduces the areas of both W1 and W3 to 45 deg^2 (the full areas are 72 deg^2 and 49 deg^2, respectively).

[3] http://www.cadc-ccda.hia-iha.nrc-cnrc.gc.ca/en/megapipe/cfhtls/index.html

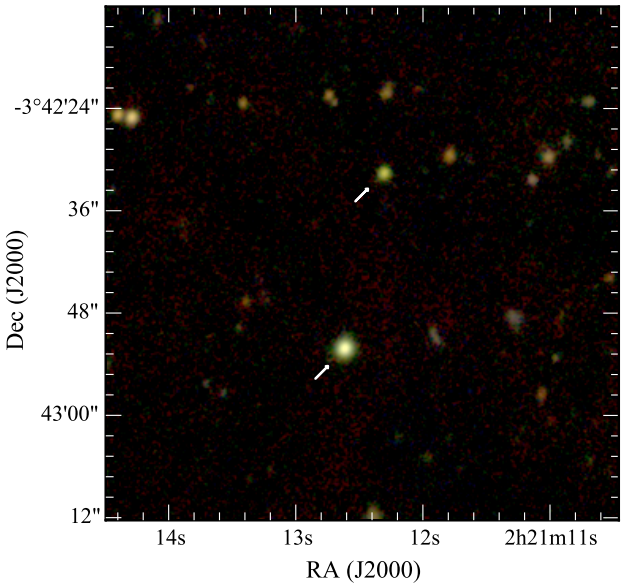

Figure 2. Color image of CFHTLS J0221-0342 generated from the CFHTLS *riz* images. The image is 1′ on a side. The two $z = 5$ quasars are indicated with arrows; in this color space they appear green relative to the redder stars and galaxies in the field (note their blue $i - z$ colors in Fig. 1). There are no well-detected galaxies between QSO-A (lower) and QSO-B (upper), and no apparent overdensity of galaxies in the vicinity. The depths of the input images are $g = 26.5$, $r = 25.9$, and $i = 25.6$ (Gwyn 2012).

After applying the morphological and quality cuts and a loose color cut of $r - i > 0.8$ the resulting density of objects is $\sim$130 deg^{-2} in the two CFHTLS fields. In order to select $z \sim 5$ quasar candidates we adapt the color criteria employed in McGreer et al. (2013) to account for the bandpass differences between the SDSS and CFHT photometric systems. This results in the following color cuts:

$$
\begin{aligned}
& S/N(u) < 2.2 \\
& S/N(g) < 2.2 \;\; \text{OR} \;\; g - r > 1.8 \\
& r - i > 1.3 \\
& i - z < 0.625((r - i) - 1.0) \\
& i - z < 0.55
\end{aligned}
$$

The resulting set of objects were visually examined and those likely to be artefacts (e.g., diffraction spikes) were rejected. In the W1 (W3) field 26 (21) objects are identified as quasar candidates to a limit of $i = 23$. When preparing our observations we noticed that two of the bright candidates had a very small separation on the sky. We examined the imaging and considered both to be viable high redshift quasar candidates, and thus prioritized them for observation. However, we emphasize that we did not search for binary candidates *a priori*; rather, we selected the objects simultaneously with identical criteria.

2.2. *MMT Observations*

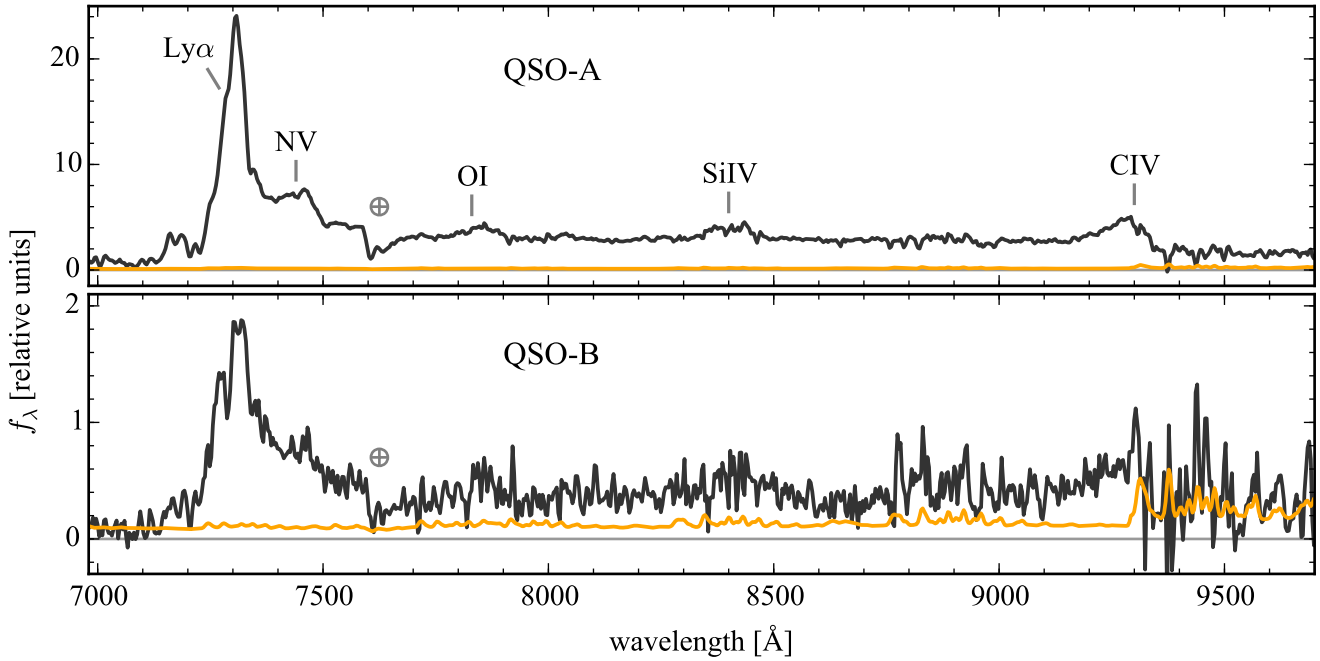

Figure 3. MMT Red Channel spectra of QSO-A (top) and QSO-B (bottom). The total integration time is 2.9 hrs. The orange lines indicate the rms noise level. The absorption feature at ∼7620 Å is telluric. The locations of prominent quasar emission lines for a redshift of $z = 5.0$ are marked in the upper panel (Lyα is offset for clarity). The spectra are remarkably similar except for the Lyα emission (see Fig. 5). The red wing of the C IV line is strongly affected by night sky emission.

We observed CFHTLS J0221-0342 with the Red Channel spectrograph (Schmidt et al. 1989) on the MMT 6.5m telescope on 2014 Jan 9, 2014 Jan 10, and 2014 Aug 28. All observations utilized a $1''\times180''$ longslit aligned at a position angle of $-12.2°$ in order to capture both quasar candidates. The objects were dispersed with the 270 mm^{-1} grating at a resolution of $R \sim 640$. For the 2014 Jan 9 observations the central wavelength was set to 7500 Å, providing wavelength coverage from 5670Å to 9290Å, and the total integration time was 70 min. For the 2014 Jan 10 and 2014 Aug 28 observations the central wavelength was 8500Å (6600Å $\lesssim \lambda \lesssim 1\mu$m) and the total integration times were 45 min. and 60 min., respectively. In all cases the seeing was marginal ($1\farcs5$ – $2''$) with non-photometric conditions.

The spectra were processed in a standard fashion with Pyraf-based scripts; details of the processing method are given in McGreer et al. (2013). Wavelength calibration was provided by an internal HeNeAr lamp, and an approximate flux calibration was obtained from observations of the spectrophotometric standard star Feige 110. The calibrations were taken immediately before the science spectra. The processed spectra from each of the three nights were interpolated onto a common linear wavelength grid and combined using inverse-variance weighting. The final spectra are displayed in Figure 3.

The spectroscopy immediately confirmed that both candidates are quasars at $z \sim 5$. In Section 3 we interpret the spectra and other available data in order to determine whether they represent two quasars at a similar redshift or gravitationally lensed images of a single source quasar.

We have obtained a total of 19 MMT spectra out of the 47 candidates with $i < 23$ in W1 and W3. A more complete analysis of this sample will be presented in a future work. Relevant to this work, we note that *all* of the observed objects are quasars at $z \gtrsim 4.5$, indicating that the color selection is highly pure. In addition, our simulations show that the color selection is highly complete (> 90%) in the range $4.75 < z \lesssim 5.15$, with a tail to ∼ 50% completeness out to $z \sim 5.4$ (see McGreer et al. 2013, for details on the simulation method). Although we have spectra for only 40% of our candidates, we consider it highly likely that any similar pair of small-separation quasars would be included in our target list, and thus we conclude that only one such pair lies within the 90 deg^2 search area to the flux limit of $i < 23$[4]. This estimate of the area of our survey (90 deg^2) will be used in §4 to infer the clustering strength of quasars at $z \sim 5$.

2.3. *Additional Observations*

CFHTLS J0221-0342 lies within the XMM-LSS (Pierre et al. 2004) survey region, and thus has a wide array of multiwavelength observations. Table 1 lists photometric observations of the quasar pair, including deep near-IR photometry from the UKIDSS Deep eXtragalactic Survey (DXS; Lawrence et al. 2007) and deep Spitzer photometry from the SWIRE survey (Lonsdale et al. 2003). The brighter quasar is also an X-ray source in the XMM-XXL survey and was included as an ancillary quasar target in the SDSS-III Baryon Oscillation Spectroscopic Survey (BOSS) Data Release 12 (Alam et al. 2015). This ancillary program[5] targeted XMM-XXL sources for spectroscopy; QSO-A was the highest redshift X-ray source in the sample, with a redshift of $z = 5.011$.

[4] We searched our candidate list for additional pairs and found two quasars with a separation of $80''$; however, they have a redshift difference of $\Delta z = 0.15$.

[5] `http://www.sdss.org/dr12/algorithms/ancillary/boss/xmmfollowup/`

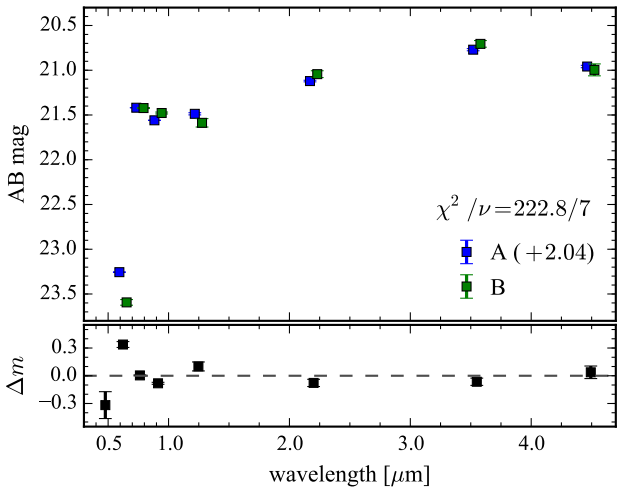

Figure 4. SEDs for QSO-A and QSO-B obtained from the CFHTLS-Wide imaging (*griz*; the *g*-band measurements are below the plot boundary in the upper panel), UKIDSS DXS (*JK*), and Spitzer/SWIRE (3.6μm and 4.5μm). The upper panel compares the photometric measurements for the two objects; the SED for QSO-A is shifted downward so that the χ^2 difference between the two SEDs is minimized. The points are offset slightly in wavelength for clarity. The lower panel shows the residual magnitude differences after the offset has been applied. There are significant differences over the full wavelength range, with the largest deviations occuring at the shortest wavelengths, where strong rest-UV emission lines contribute significantly to the fluxes. The photometry of both objects is always simultaneous due to their proximity, minimizing any differences arising from variability. All points include error bars, but they are generally smaller than the symbol size.

Table 1
Properties of the binary quasar.

	QSO-A	QSO-B
RA (J2000)	02:21:12.613	02:21:12.315
Dec (J2000)	-03:42:52.19	-03:42:31.64
g	24.104 ± 0.029	25.822 ± 0.142
r	21.221 ± 0.004	23.594 ± 0.032
i	19.383 ± 0.001	21.423 ± 0.005
z	19.524 ± 0.002	21.478 ± 0.011
J	19.452 ± 0.012	21.588 ± 0.047
K	19.086 ± 0.009	21.044 ± 0.038
3.6μm	18.735 ± 0.012	20.705 ± 0.037
4.5μm	18.923 ± 0.013	20.996 ± 0.067
5.8μm	19.248 ± 0.073	-
8.0μm	18.825 ± 0.046	-
24μm	17.090 ± 0.051	-

Note. — All photometry is on the AB system and corrected for Galactic extinction.

It is important to note that although CFHTLS J0221-0342 happens to lie within a deep extragalactic survey field, for our survey it was selected based on optical colors from the CFHTLS-Wide alone.

3. A QUASAR PAIR OR A LENS?

We first consider whether CFHTLS J0221-0342 represents a binary quasar or a pair of gravitationally lensed images of a single source at $z = 5$. Because lensing is achromatic, if they are lensed images the two objects should present similar colors at all wavelengths. There are two important effects that can affect the observed colors: 1) differential reddening along the independent light paths to the two images, and 2) time delays between the lensed images combined with intrinsic source variability. Figure 4 presents the multiwavelength SEDs of CFHTLS J0221-0342, where deviations as large as $\sim$30% from the mean flux offset are present across a wide range of wavelengths. These differences are far greater than the photometric uncertainties, which are $< 1\%$ from *g*-band to *K*-band. The statistical uncertainties are appropriate here since the photometry represents *relative* flux measurements between the two objects, as the same calibrations have been applied to both objects. In addition, because of their proximity, the photometry of the two objects is always simultaneous, minimizing any differences arising from intrinsic source variability. We apply the χ^2 statistic given by Hennawi et al. (2006, their equation 2) to the two SEDs as a test of the hypothesis that a simple flux scaling combined with photometric scatter accounts for their differences (i.e., they are lensed images) and rule this out at high significance, obtaining $\chi^2/\nu = 223/7$ from the multiwavelength SEDs[6]. Finally, there is no trend in the flux differences that would be consistent with reddening.

The MMT spectra of the two objects are highly similar to the level of the *S*/*N* and resolution available. We obtain a small redshift difference from fitting the O I emission line in the MMT spectra; Gaussian fits with the IRAF *splot* command return $z(\mathrm{A}) = 5.016$ and $z(\mathrm{B}) = 5.019$, a difference of $\approx 160\,\mathrm{km\,s^{-1}}$. However, the O I line is weakly detected in the QSO-B spectrum and the uncertainty on the line centroid is $\approx 300\,\mathrm{km\,s^{-1}}$, thus this difference is not significant. The Lyα lines are detected at high *S*/*N* in both spectra and the line profiles in the wings are nearly identical (Fig. 5), agreeing to within two spectral pixels, or $\lesssim 270\,\mathrm{km\,s^{-1}}$. As it is difficult to conclusively state the velocity offset between the two spectra, in the rest of this work we adopt the difference obtained from the O I fits, $\Delta z \lesssim 0.03$.

There are differences between the two spectra that indicate they are not likely to originate from a single source quasar. QSO-B has a clear absorption feature just blueward of Lyα at $\sim$7286Å while QSO-A has a transmission peak at $\sim$7170Å; both of these features are significantly weaker in the opposite spectrum (Figure 5). Also, the N V emission from QSO-A is greater than that from QSO-B.

Another consideration is that a configuration that produces a large separation (21″) image pair of a $z = 5$ quasar is highly unlikely; only three large-separation lensed quasar systems are known in the entire SDSS (Inada et al. 2003; Dahle et al. 2013; Rusu et al. 2013). Large separations can arise from group- or cluster-scale lens masses. For this configuration, the peak in the expected lens redshift distribution is at $z \sim 0.7$ and the probability of a source quasar at $z = 5$ with an image separation $> 20''$ is extremely small (Hennawi et al. 2007; Li et al. 2007). Furthermore, the CFHTLS imaging is

[6] Hennawi et al. (2006) obtain a median value of $\chi^2/\nu = 33.1/4$ for a sample of SDSS quasars at $2.4 < z < 2.45$; the expectation for lensed images in the absence of differential reddening is $\chi^2/\nu \sim 1$. To compute this value we use the photometry from *g* through 4.5μm where both objects are well detected, hence the 7 degrees of freedom. If we restrict the data to the *griz* bands to better compare with the SDSS data, we obtain $\chi^2/\nu = 212/3$.

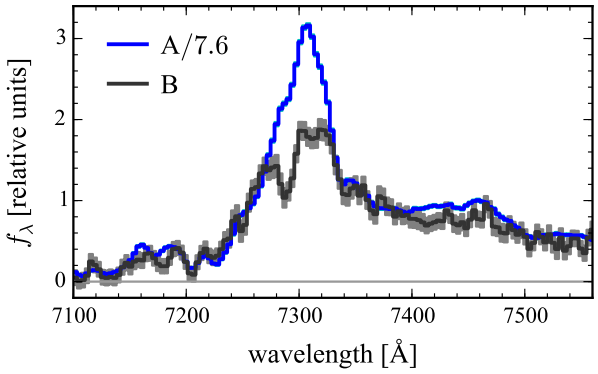

Figure 5. Lyα emission line profiles for QSO-A (blue) and QSO-B (dark gray). The rms noise is shown as shaded regions (for QSO-A it is roughly the same as the line width). The QSO-A spectrum has been rescaled by the continuum flux ratio between the two objects at 8200Å. The Lyα emission from QSO-A has larger equivalent width, as does the N V emission line at 7440Å (note that the QSO-B spectrum has a redder continuum slope, consistent with its redder $r - i$ color, see Fig. 1). The Lyα emission of QSO-B has stronger absorption features. The wings of the two lines are nearly identical, indicating that the velocity offset is extremely small; it is $\lesssim 2$ pixels or $\lesssim 270$ km s^{-1}.

sufficiently deep that a group-scale overdensity at $z < 1$ should be immediately apparent in the optical imaging, but as Figure 2 shows, there are no galaxies detected between QSO-A and QSO-B, and no obvious overdensity of galaxies in the vicinity.

In conclusion, the mismatched SEDs of the two objects and the lack of any obvious foreground mass to generate a wide separation lens configuration strongly argue against the lens hypothesis for this pair of objects. We proceed to interpret them as a binary quasar.

4. IMPLICATIONS FOR QUASAR CLUSTERING AT $Z > 5$

Quasars peak as a luminous population near $z \sim 2.5$, and bright quasars at higher redshift are increasingly rare (Richards et al. 2006). Combining the depth and area necessary to survey large numbers of $z \sim 5$ quasars is therefore taxing. Due to the difficulty in studying a significant quantity of quasars at high redshift, quasar clustering has only been measured in a statistical fashion out to $z \sim 4$, by Shen et al. (2007), who found a correlation length of $r_0 \sim 24h^{-1}$ Mpc. This level of clustering is considered "large," in the sense that it is at the limits of what might be predicted by theoretical models that use the luminosity function to infer quasar clustering (e.g. Hopkins et al. 2007) and in the sense that clustering measurements at $z \sim 2.5$ typically obtain significantly smaller values of $r_0 \sim 8h^{-1}$ Mpc (e.g. White et al. 2012; Eftekharzadeh et al. 2015). That r_0 seems large at $z \sim 4$ motivates further measurements of quasar clustering to determine if r_0 remains large at comparable or higher redshifts.

A small number of close quasar pairs can be used as an alternative method for quantifying the clustering of high redshift quasars. In the absence of clustering it would be extraordinarily unlikely to find multiple quasars within a small cosmological volume, hence pairs can be used to infer the clustering strength required to increase the likelihood of companion quasars with small separations. An example of this approach is that of Schneider et al. (2000), who used a single binary quasar at $z = 4.25$ separated by $\Delta\theta = 33.4''$ on the plane of the sky to infer $r_0 \sim 12$–30 Mpc for the correlation length of $z \sim 4$ quasars, presaging the Shen et al. (2007) estimate of $r_0 \sim 24h^{-1}$ Mpc. In our chosen cosmology, the transverse projected separation of the Schneider et al. (2000) quasar pair is $160h^{-1}$ kpc compared to $90h^{-1}$ kpc ($\Delta\theta = 21''$; $z = 5.02$) for the pair we have discovered.

In this section we use our binary quasar to estimate r_0 for quasars at $z \sim 5$. It may be helpful to remember that at $z = 5$, an angle of $1''$ subtends a transverse separation of $26h^{-1}$ kpc comoving ($4.35h^{-1}$ kpc proper).

4.1. *The luminosity function*

The significance of observing a close pair of quasars relative to random chance is determined from the QLF. We adopt the recent measurement of the QLF at $z = 5$ from McGreer et al. (2013) based on quasars drawn from the SDSS Stripe 82 region, extending to a depth of $i = 22$. Although CFHTLS J0221-0342 is drawn from a deeper survey ($i < 23$) and thus requires extrapolation from the McGreer et al. (2013) results, it is worth noting that both quasars have $i < 22$ and are thus within the range of the Stripe 82 measurement.

The QLF is typically fit with a double power-law form,

$$\Phi(M, z) = \frac{\Phi^*(z)}{10^{0.4(\alpha+1)(M-M^*)} + 10^{0.4(\beta+1)(M-M^*)}} \ . \quad (1)$$

McGreer et al. (2013) estimate the characteristic luminosity to be $M^* = -27.21$ and the faint and bright end slopes to be $\alpha = -2.03$ and $\beta = -4.0$, respectively. The parameter Φ^* is best described by a term that evolves with redshift, $\log \Phi^*(z) = \log \Phi^*(z = 6) + k(z - 6)$, with $\log \Phi^*(z = 6) = -8.94$ and k $= -0.47$ (see §6 of McGreer et al. 2013 for a detailed discussion on the fitting procedure and redshift evolution of the QLF parameters).

As noted in §2, our survey of $z \sim 5$ quasars has progressed such that it is reasonable to assume our binary quasar is drawn from a complete survey covering 90 deg^2 to a flux limit of $i < 23$. The number density of quasars brighter than $i' = 23$ in our survey is calculated by taking the integral of the QLF between the k-corrected absolute magnitudes, $M_i^{\rm bright}$ and $M_{i'}$, corresponding to the bright and faint end of the apparent magnitude range of our survey:

$$n(z, i < i') = \int_{M_i^{\rm bright}}^{M_{i'}} dM_i \ \Phi(M_i, z). \quad (2)$$

We use a constant k-correction of $k_{\rm corr} = -2.2$, which is reasonable over the full redshift range of interest (see Fig. 6 of McGreer et al. 2013). The number densities obtained from the QLF are relatively insensitive to the bright limit (in apparent magnitude) adopted for the integration. We ignore the incompleteness due to our selection efficiency, which would reduce the observed number densities. We stress that this makes our measurements more conservative, in that any incompleteness in our survey would *increase* the inferred clustering signal, as we would be more likely to have missed additional close pairs. The QLF predicts ~ 0.9 deg^2 quasars over the redshift range $4.7 < z < 5.2$, which already hints that a quasar pair separated by $21''$ at $z \sim 5$ would be highly unusual if quasars were not significantly clustered at high redshift.

4.2. *Estimating the Correlation Length Using the Schneider et al. (2000) Formalism*

Following Schneider et al. (2000) we determine the correlation length of quasars by comparing the single pair we have found to the number of pairs we would expect to find in the volume enclosing our pair. The mean number expected in a given volume can be determined from the QLF. The odds of finding two quasars in that volume (corresponding to our binary quasar) can then be determined from the Poisson distribution, as Poisson statistics are an excellent model for quasar clustering on small scales where the pairs are independent (e.g. Myers et al. 2006). The correlation length can be related to the excess clustering over random as

$$\frac{N}{N_{\rm rand}} = \frac{\int_0^R 4\pi r^2 \xi(r)\ dr}{\int_0^R 4\pi r^2\ dr} = \frac{3}{3-\gamma}\left(\frac{R}{r_0}\right)^{-\gamma}|_{\gamma=2} = 3\left(\frac{R}{r_0}\right)^{-2} , \quad (3)$$

where we have adopted a power-law form of $\xi(r) = (r/r_0)^{-\gamma}$ with $\gamma = 2$ for the slope of the correlation function, as used in many studies of the clustering of quasars at high redshift on large and small scales (e.g. Shen et al. 2010; White et al. 2012; Eftekharzadeh et al. 2015).

As it is unclear *a priori* to what degree the redshift difference between the components of our binary quasar is due to line-of-sight separation versus infall, we will calculate "minimum," "medium" and "maximum" separations based on the transverse and line-of-sight comoving separations of our pair (again following Schneider et al. 2000). Our quasar pair is at $z = 5.02$, is separated by $21''$ on the plane of the sky, and has a redshift difference of $\Delta z \lesssim 0.03$. If the separation of the quasars is entirely in the transverse direction, then the components of our pair are separated by 810 kpc comoving (the "minimum" separation). If the full redshift difference is also due to physical separation, then the components of our pair are separated by 16.1 Mpc comoving (the "maximum" separation). If half of the redshift difference is attributable to physical separation, then the components of our pair are separated by 8.08 Mpc comoving (the "medium" separation).

Integrating the McGreer et al. (2013) QLF to a limit of $i = 23$ over the redshift range $4.7 < z < 5.2$ results in a number density of $\approx 1.75 \times 10^{-7}\,{\rm Mpc}^{-3}$, ignoring selection completeness. Our "minimum" separation of 810 kpc implies a quasar pair embedded in a volume of $2.25\,{\rm Mpc}^3$. Multiplying this by the number density yields an expectation of 3.9×10^{-7} quasars in the volume of interest. Assuming a Poisson distribution, the probability of two quasars lying within this volume is 7.3×10^{-3} for an all-sky survey. As our survey only encompasses $90\,{\rm deg}^2$, the odds of finding the binary quasar within our survey are 1 in 62,400, implying that this discovery would have been extremely unlikely in the absence of clustering. Substituting $N/N_{\rm rand} = 62{,}400$ and $R = 810$ kpc into Eqn. 3 implies $r_0 = 117$ Mpc, or $r_0 = 74h^{-1}$ Mpc.

Similar logic implies $r_0 = 25h^{-1}$ Mpc for our "medium" separation case and $r_0 = 18h^{-1}$ Mpc for our "maximum" separation case. Thus our expectation is that $r_0 \sim 25h^{-1}$ Mpc for quasars at $z \sim 5$, with a lower-bound of $r_0 \sim 18h^{-1}$ Mpc. If we adopt a shallower slope for the power law index the correlation length would need to be even greater; e.g., for $\gamma = 1.8$ the "medium" separation case results in $r_0 \sim 33h^{-1}$ Mpc. Our measurement implies that the amplitude of quasar clustering at $z \sim 5$ is similar to that measured at $z \sim 4$ by Shen et al. (2007).

4.3. *Estimating the Correlation Length Using the Hennawi et al. (2006) Formalism*

The Schneider et al. (2000) formalism is simple and straightforward. However, by selecting "minimum" and "maximum" extremes for the distribution of peculiar velocities in the redshift-space direction this method ignores our expectation for this distribution. In particular, the "minimum" case applies if the two quasars are at the same distance and any redshift difference is due to the local velocity field. This is a reasonable assumption in our case; however, it is useful to characterize the uncertainty on that difference, and for that we turn to the method of Hennawi et al. (2006). This method accounts for a realistic peculiar velocity distribution for the quasars so that we can place a more formal (Poisson) error on the correlation length we infer from the existence of the binary.

Following the method described in Hennawi et al. (2006), we assume that binary quasars are well-described by a maximum possible peculiar velocity of $|v_{\rm max}| = 2000\,{\rm km\,s^{-1}}$. We then project the redshift-space correlation function over this velocity interval,

$$w_p(R,z) = \int_{-v_{\rm max}/aH(z)}^{v_{\rm max}/aH(z)} \xi_s(R,s,z) ds\ , \quad (4)$$

where $H(z)$ is the expansion rate at redshift z and ξ_s is the redshift-space quasar correlation function. We include the cosmological scale factor $a = 1/(1+z)$ to convert distances to comoving units.

Given that we are working with a single pair embedded in a relatively large volume, w_p could be highly sensitive to changes in the model correlation function with scale and/or redshift. Again following Hennawi et al. (2006) we ameliorate this effect by measuring the volume-averaged correlation function $\bar{W}_p(z)$ over the entire radial bin of comoving distance that corresponds to the transverse separation of our binary quasar $[R_{\rm min}, R_{\rm max}]$. This results in

$$\bar{W}_p(z) = \frac{\int_{-\frac{v_{\rm max}}{aH(z)}}^{\frac{v_{\rm max}}{aH(z)}} \int_{R_{\rm min}}^{R_{\rm max}} \xi_s(R,s,z) 2\pi R dR ds}{V_{\rm shell}}\ , \quad (5)$$

where $V_{\rm shell}$, the volume of a cylindrical shell in redshift space, is given by

$$V_{\rm shell} = \pi\left(R_{\rm max}^2 - R_{\rm min}^2\right)\left[\frac{2v_{\rm max}}{aH(z)}\right]\ . \quad (6)$$

Although the redshift-space correlation function is a convolution of the real-space correlation function with the distribution of peculiar velocities, we are projecting over a volume large enough to contain the full extent of this distribution function. Hence it is a reasonable approximation to replace the redshift-space correlation function $\xi_s(R,s,z)$ with its real-space counterpart $\xi(r,z)$ where $\xi(r) = (r/r_0)^{-\gamma}$ and $r^2 = R^2 + x^2$. We adopt $\gamma = 2$

for the real-space correlation function, as explained in §4.2, and assume that this form remains valid for all redshifts of interest (i.e. $\xi(r, z) = \xi(r)$). The integral in eqn. 5 is instead conducted along the line-of-sight distance x,

$$\bar{W}_p(R_{\rm min}, R_{\rm max}, z) = \frac{\int_{-\frac{v_{\rm max}}{aH(z)}}^{\frac{v_{\rm max}}{aH(z)}} \int_{R_{\rm min}}^{R_{\rm max}} \left(\frac{x^2+R^2}{{r_0}^2}\right)^{-\frac{\gamma}{2}} 2\pi R dR dx}{V_{\rm shell}} . \quad (7)$$

We adopt $[R_{\rm min}, R_{\rm max}] = [25, 550]h^{-1}\,{\rm kpc}$ (i.e. [40, 810] kpc). Here, $R_{\rm max}$ corresponds to the $21''$ separation of our binary quasar at $z = 5.02$. We set $R_{\rm min}$ to correspond to $1''$, below which the seeing in the CFHTLS imaging we used for target selection would have precluded the selection of a pair of quasars. The number of expected companions of any individual quasar in our survey as a function of transverse separation and redshift is then

$$N_c = n(4.7 < z < 5.2, i < 23) \times V_{\rm shell}\,[1 + \bar{W}_p(25, 550, z)] , \quad (8)$$

where n is given by our adopted QLF (see Eqn. 2). By varying the correlation length in Eqn. 7 we obtain a range of model values for the number of companions we expect at a separation of $21''$ within our survey volume at $z = 5.02$. We then compare the predicted number of companions to the discovery of a single binary out of a sample of 47 quasar candidates,[7] i.e., within our sample of 47 quasars there are two objects within the cylindrical shell defined by $V_{\rm shell}$. Thus we are seeking a model for the correlation function that results in the expected number of companions to be $N_c = 2/47 = 0.04255$.

We find the correlation length that best describes our binary quasar is $86h^{-1}\,{\rm Mpc}$, with a 1σ lower bound of $25h^{-1}\,{\rm Mpc}$. The lower bound has been determined using the confidence interval for a single measurement provided by Gehrels (1986).

As with the analysis in §4.2, this result depends on our adopted QLF and that our assumed form of the correlation function is valid and non-evolving across our redshift range of interest. In particular, in calculating an r_0 that is significantly larger than the scales probed by our pair, we are implicitly assuming that clustering at small scales can be extrapolated to large scales[8] (as was found to be the case for low-z quasars by Kayo & Oguri 2012 and consistent with results at $z \sim 3$–4 from Shen et al. 2010). Whether we employ the Hennawi et al. (2006) formalism or the Schneider et al. (2000) formalism, we find that the existence of this binary quasar implies a correlation length $r_0 > 20h^{-1}\,{\rm Mpc}$, consistent with the $r_0 \sim 25h^{-1}\,{\rm Mpc}$ measured at $z \sim 4$ by Shen et al. (2007). This strongly suggests that quasars are at least as clustered at $z \sim 5$ as has been found at $z \sim 4$.

[7] We ignore the fact that we do not have spectroscopic confirmation for all of our candidates. First, as mentioned in §2.2, we consider our survey to be highly complete to small-separation pairs. Second, our spectroscopy has shown that our color selection is highly pure, so that we expect nearly all of the 47 candidates to be $z \sim 5$ quasars. It is more conservative to use the full candidate sample, as including only the objects with spectroscopy would greatly *increase* the implied clustering signal. In addition, the binary reported here was prioritized for observation, so it is more correct to adopt the full sample.

[8] It is worth noting that the projected separation of our binary is just at the scale at which the two-halo term begins to contribute to the projected correlation function in the HOD models of Kayo & Oguri (2012); see their Fig. 6.

5. CONCLUSIONS

We have discovered a pair of quasars with apparently identical redshifts of $z = 5.02$ and a separation of $21''$ on the sky. A number of factors argue against the pair being gravitationally lensed images of a single source quasar. These include differences in spectral profiles and SED shapes, and the fact that no deflector is present between the two quasars in relatively deep optical imaging. Assuming the quasar pair is a binary, the small projected separation (135 kpc proper) and lack of a clear redshift offset implies their physical separation is quite small, within a factor of $\sim$ 2–3 of the virial radius of a typical quasar-hosting dark matter halo at high redshift ($\sim 10^{12}$–$10^{13}\ M_\odot$, Hopkins et al. 2007; Shen et al. 2007; White et al. 2012; Eftekharzadeh et al. 2015). This single detection of a binary at $z = 5$ favors models where quasars are strongly clustered at high redshift, at least on small scales.

The clustering of quasars is sensitive not only to the triggering mechanism(s), but also feedback effects that terminate black hole growth. Globally, the quasar population experiences a "downsizing" trend at $z \lesssim 3$, as activity shifts to lower mass and lower luminosity systems (e.g., Ross et al. 2013). This is often thought to be due to feedback, as the most massive systems form early but rapidly shut down after their quasar phase, freezing their black hole mass while the host halos continue to grow. At high redshift the picture is murkier, with few constraints on the black hole mass and Eddington ratio distributions. This is demonstrated by Hopkins et al. (2007), who compare three disparate models for the continued growth of black holes at high redshift after their luminous quasar phase. If feedback is efficient at high redshift, the correlation length should decrease strongly with increasing redshift. If feedback is inefficient such that the black holes grow continuously until $z \sim 2$, the correlation length flattens out at high redshift. If quasars grow at the same rate as their host halos at $z > 3$ (the "maximal" growth model), the correlation length rises sharply, implying that quasars at $z = 5$ are more strongly clustered by a factor of a few compared to the measurements at $z \sim 2.5$.

While repeating the caveat that we have only measured small-scale clustering from a single, high-luminosity binary at $z = 5$, this observation is most consistent with a large correlation length, favoring the models in which feedback is highly inefficient. Indeed, Willott et al. (2010) find that the Eddington ratios of $z \sim 6$ quasars are near unity across a range of luminosities, suggesting that fainter quasars are not in a "decaying" phase of black hole growth.

It is surprising to have found two highly luminous quasars — presumably powered by $> 10^8\ M_\odot$ black holes and situated in massive dark matter halos — in such close proximity at this redshift. Previous searches have relied on wide-area surveys such as the SDSS, whereas we surveyed only $\sim 0.1\%$ of the sky and yet discovered a $z = 5$ binary quasar *bright enough to have been selected from*

SDSS imaging. Whether this was simply a chance find will await a more comprehensive search for quasar pairs at $z \gtrsim 5$.

Measurements of high-redshift quasar clustering on large scales are crucial to discriminating between feedback models and better understanding the early growth of the most massive black holes in the universe. Such measurements are just possible today with wide-area, medium-depth fields such as SDSS Stripe 82 and the CFHTLS, and ongoing surveys such as the DES, the DESI Imaging Surveys (DECaLS, BASS, and MzLS), and KIDS also provide the requisite combination of depth and area. Obtaining a fully three-dimensional clustering measurement demands a considerable investment in spectroscopic follow-up given the low sky density; however, if quasars do cluster strongly at high redshift (as implied by our observations), a dense survey over a relatively small area could produce a statistically meaningful result.

IDM and XF acknowledge support from NSF grants 11-06682 and NSF 15-15115. ADM and SE were supported in part by NASA ADAP award NNX12AE38G and by NSF awards 12-11112 and 15-15404. This research made use of Astropy, a community-developed core Python package for Astronomy (Astropy Collaboration et al. 2013). Observations reported here were obtained at the MMT Observatory, a joint facility of the Smithsonian Institution and the University of Arizona. Also based on observations obtained with MegaPrime/MegaCam, a joint project of CFHT and CEA/DAPNIA, at the Canada-France-Hawaii Telescope (CFHT) which is operated by the National Research Council (NRC) of Canada, the Institut National des Science de l'Univers of the Centre National de la Recherche Scientifique (CNRS) of France, and the University of Hawaii. The observations at the Canada-France-Hawaii Telescope were performed with care and respect from the summit of Maunakea which is a significant cultural and historic site. This work is based in part on data products produced at the Canadian Astronomy Data Centre as part of the Canada-France-Hawaii Telescope Legacy Survey, a collaborative project of NRC and CNRS.

Facilities: MMT (Red Channel spectrograph), CFHT (MegaCam)

REFERENCES

Alam, S. et al. 2015, ApJS, 219, 12
Astropy Collaboration et al. 2013, A&A, 558, A33
Bertin, E. & Arnouts, S. 1996, A&AS, 117, 393
da Ângela, J., Shanks, T., Croom, S. M., et al. 2008, MNRAS, 383, 565
Dahle, H., Gladders, M. D., Sharon, K., et al. 2013, ApJ, 773, 146
Eftekharzadeh, S., Myers, A. D., White, M., et al. 2015, MNRAS, 453, 2779
Gehrels, N. 1986, ApJ, 303, 336
Gwyn, S. D. J. 2012, AJ, 143, 38
Hennawi, J. F., Dalal, N., & Bode, P. 2007, ApJ, 654, 93
Hennawi, J. F., Myers, A. D., Shen, Y., et al. 2010, ApJ, 719, 1672
Hennawi, J. F., Strauss, M. A., Oguri, M., et al. 2006, AJ, 131, 1
Hopkins, P. F., Lidz, A., Hernquist, L., Coil, A. L., Myers, A. D., Cox, T. J., & Spergel, D. N. 2007, ApJ, 662, 110
Inada, N., Oguri, M., Pindor, B., et al. 2003, Nature, 426, 810
Kayo, I. & Oguri, M. 2012, MNRAS, 424, 1363
Lawrence, A., Warren, S. J., Almaini, O., et al. 2007, MNRAS, 379, 1599
Li, G. L., Mao, S., Jing, Y. P., Lin, W. P., & Oguri, M. 2007, MNRAS, 378, 469
Lidz, A., Hopkins, P. F., Cox, T. J., Hernquist, L., & Robertson, B. 2006, ApJ, 641, 41
Lonsdale, C. J. et al. 2003, PASP, 115, 897
McGreer, I. D., Jiang, L., Fan, X., et al. 2013, ApJ, 768, 105
Myers, A. D., Brunner, R. J., Richards, G. T., et al. 2006, ApJ, 638, 622
Myers, A. D., Richards, G. T., Brunner, R. J., et al. 2008, ApJ, 678, 635
Oke, J. B. & Gunn, J. E. 1983, AJ, 266, 713
Pierre, M. et al. 2004, **??**jnlJ. Cosmology Astropart. Phys., 2004, 011
Planck Collaboration et al. 2015, ArXiv e-prints
Richards, G. T., Strauss, M. A., Fan, X., et al. 2006, AJ, 131, 2766
Ross, N. P., McGreer, I. D., White, M., et al. 2013, ApJ, 773, 14
Rusu, C. E., Oguri, M., Iye, M., et al. 2013, ApJ, 765, 139
Schlegel, D. J., Finkbeiner, D. P., & Davis, M. 1998, ApJ, 500, 525
Schmidt, G. D., Weymann, R. J., & Foltz, C. B. 1989, PASP, 101, 713
Schneider, D. P., Fan, X., Strauss, M. A., et al. 2000, AJ, 120, 2183
Shen, Y., Hennawi, J. F., Shankar, F., et al. 2010, ApJ, 719, 1693
Shen, Y., McBride, C. K., White, M., et al. 2013, ApJ, 778, 98
Shen, Y., Strauss, M. A., Oguri, M., et al. 2007, AJ, 133, 2222
Shen, Y., Strauss, M. A., Ross, N. P., et al. 2009, ApJ, 697, 1656
White, M., Myers, A. D., Ross, N. P., et al. 2012, MNRAS, 424, 933
Willott, C. J., Albert, L., Arzoumanian, D., et al. 2010, AJ, 140, 546